Acta Oceanol. Sin., 2021, Vol. 40, No. 11, P. 50–61
https://doi.org/10.1007/s13131-021-1765-7
http://www.aosocean.com
E-mail: ocean2@hyxb.org.cn

Effects of the seasonal variation in chlorophyll concentration on sea surface temperature in the global ocean

Jinfeng Ma[1], Hailong Liu[1, 2*], Pengfei Lin[1, 2], Haigang Zhan[3, 4]

[1] State Key Laboratory of Numerical Modeling for Atmospheric Sciences and Geophysical Fluid Dynamics, Institute of Atmospheric Physics, Chinese Academy of Sciences, Beijing 100029, China

[2] College of Earth and Planetary Sciences, University of Chinese Academy of Sciences, Beijing 100049, China

[3] Southern Marine Science and Engineering Guangdong Laboratory (Guangzhou), Guangzhou 511458, China

[4] State Key Laboratory of Tropical Oceanography, South China Sea Institute of Oceanology, Chinese Academy of Sciences, Guangzhou 510301, China

Received 19 October 2020; accepted 24 November 2021

Abstract

The effects of biological heating on the upper-ocean temperature of the global ocean are investigated using two ocean-only experiments forced by prescribed atmospheric fields during 1990–2007, on with fixed constant chlorophyll concentration, and the other with seasonally varying chlorophyll concentration. Although the existence of high chlorophyll concentrations can trap solar radiation in the upper layer and warm the surface, cooling sea surface temperature (SST) can be seen in some regions and seasons. Seventeen regions are selected and classified according to their dynamic processes, and the cooling mechanisms are investigated through heat budget analysis. The chlorophyll-induced SST variation is dependent on the variation in chlorophyll concentration and net surface heat flux and on such dynamic ocean processes as mixing, upwelling and advection. The mixed layer depth is also an important factor determining the effect. The chlorophyll-induced SST warming appears in most regions during the local spring to autumn when the mixed layer is shallow, e.g., low latitudes without upwelling and the mid-latitudes. Chlorophyll-induced SST cooling appears in regions experiencing strong upwelling, e.g., the western Arabian Sea, west coast of North Africa, South Africa and South America, the eastern tropical Pacific Ocean and the Atlantic Ocean, and strong mixing (with deep mixed layer depth), e.g., the mid-latitudes in winter.

Key words: sea surface temperature, heat budget, upwelling, mixing, biological heating

Citation: Ma Jinfeng, Liu Hailong, Lin Pengfei, Zhan Haigang. 2021. Effects of the seasonal variation in chlorophyll concentration on sea surface temperature in the global ocean. Acta Oceanologica Sinica, 40(11): 50–61, doi: 10.1007/s13131-021-1765-7

1 Introduction

Marine phytoplankton plays a key role in the global biogeochemical system and can modulate the upper ocean temperature. Phytoplankton in the ocean could trap solar radiation in the upper mixed layer, resulting in surface warming, subsurface cooling, and mixed layer shoaling (Lewis et al., 1983, 1990; Sathyendranath et al., 1991; Siegel et al., 1995). Lewis et al. (1983) observed that the vertical distribution of chlorophyll concentration could impact the heating rate at different depths, and the heating rate decreases with increasing depth. Siegel et al. (1995) observed that a bloom event in the western Pacific reduced the net solar flux 6 W/m^2 at a depth of 30 m and increased the upper mixed layer heating rate by 0.11°C per month. Biological heating significantly impacts the upper ocean temperature and atmospheric processes (Wetzel et al., 2006; Ballabrera-Poy et al., 2007; Lengaigne et al., 2007; Löptien et al., 2009; Gnanadesikan and Anderson, 2009; Jochum et al., 2010; Ma et al., 2015; Zhang, 2015; Kang et al., 2017; Zhang et al., 2018, 2019; Tian et al., 2020).

Biological heating effects are closely related to ocean dynamics, e.g., upwelling. Nakamoto et al. (2001) showed that chlorophyll pigments in the eastern equatorial Pacific upwelling region can lead to decreased sea surface temperature (SST) due to the upwelling cold water caused by a strengthened equatorial undercurrent and increased subsurface convergence. Anderson et al. (2007) suggested that chlorophyll is implicated in the maintenance of the Pacific cold tongue. The chlorophyll in the off-equatorial region affects the SST more than that in the equatorial region. Lin et al. (2007) reported similar results that the enhanced upward velocity in the eastern tropical Pacific is mainly caused by the horizontal gradient of the chlorophyll concentration, which enhances the horizontal gradient of the upper ocean temperature and strengthens the circulation. A lower SST combines with the cooled water below the mixed layer. Liu et al. (2012a) and Ma et al. (2012, 2014) investigated the biological effects in the upwelling regions in the eastern tropical Indian Ocean, South China Sea and western Arabian Sea, respectively. They also ob-

Foundation item: The National Key R&D Program for Developing Basic Sciences under contract Nos 2018YFA0605703, 2016YFC1401601 and 2016YFC1401401; the National Natural Science Foundation of China under contract Nos 41931182, 41931183, 41976026 and 41776030; the State Key Laboratory of Tropical Oceanography, South China Sea Institute of Oceanology, Chinese Academy of Sciences Program under contract No. LTO1912; the Key Special Project for Introduced Talents Team of Southern Marine Science and Engineering Guangdong Laboratory (Guangzhou) under contract No. GML2019ZD0305.
*Corresponding author, E-mail: lhl@lasg.iap.ac.cn

served decreased SST and strengthened upwelling in boreal summer when upwelling occurs. There have been contradictory results of a warming SST in the eastern equatorial Pacific (Murtugudde et al., 2002; Marzeion et al., 2005). The inconsistency is related to the radiation scheme in the control experiment and biological experiment. The shortwave penetration depth impacts the heat transport and large ocean circulation (Sweeney et al., 2005). Murtugudde et al. (2002) use a constant depth of 17 m as a reference, which is shallower than the attenuation depth in the biological experiment. As a result, they determined a warming effect in the equatorial Pacific. In contrast, Nakamoto et al. (2001) used a constant depth of 23 m in the control, which is deeper than the attenuation depth in the biological experiment, and obtained a cooling effect. Such inconsistent results reflect our insufficient knowledge of the subject and need for more studies to be conducted.

In addition to upwelling, other factors can affect biological heating effect, such as the structure of the mixed layer or level of convective mixing. Wu et al. (2007) demonstrated that biological heating is impacted by both the chlorophyll concentration and the mixed layer depth (MLD). The SST increases by more than 1°C in summer and autumn with the existence of chlorophyll but is negligible in winter and spring when the MLD is very thick in the Labrador Sea. Ma et al. (2014) found that strong convective mixing in the northern Arabian Sea in winter could also impact biological heating. Compared to the control experiment, the biological experiment brought much colder subsurface water to the surface and cooled the SST. Thus, the effect of the convective mixing is similar to that of the upwelling, which can bring cold water from below the mixed layer up to the surface layer.

Notably, most studies on the effects of biological heating have been confined to the tropics and subtropics, e.g., the eastern tropical Pacific Ocean, and the western and eastern tropical Indian Ocean. Little attention has been paid to other regions, especially those in the Southern Hemisphere and mid-latitudes, where the chlorophyll concentrations are also high. In the mid-latitude regions, chlorophyll concentrations show strong seasonal variation, with high values in local spring, summer and autumn and low values in local winter (Fig. 1). The effects of biological heating in these regions and its seasonal variability are not properly understood. Therefore, the purpose of the present study is to examine the biological heating effects at the global scale. We chose several special regions globally and sorted them into different groups according to the heat budget analysis in the global ocean (60°S–60°N). The differences in these groups' responses to chlorophyll heating and the associated changes in ocean dynamics and thermodynamics are explored. The potential impacts for the global climate are also discussed.

2 Model and data

2.1 *Observational data*

Satellite-retrieved chlorophyll concentration data from the Sea-viewing Wide Field-of-view Sensor (SeaWiFS) (http://oceandata.sci.gsfc.nasa.gov/SeaWiFS/Mapped/Monthly/9km/chlor/) are used in the present study to analyze the attenuation depth and as a model input. The data are monthly and cover the period from September 1997 to December 2007; the horizontal resolution is 0.25°. There are some missing chlorophyll concentration data for high latitudes in local winter, so these were interpolated via Kriging interpolation. The climatological ocean temperatures and salinities are from World Ocean Atlas 2013 (WOA13) (Locarnini et al., 2013), with a resolution of 1° × 1°. The forcing of the ocean model comes from the Corrected Inter-Annual Forcing

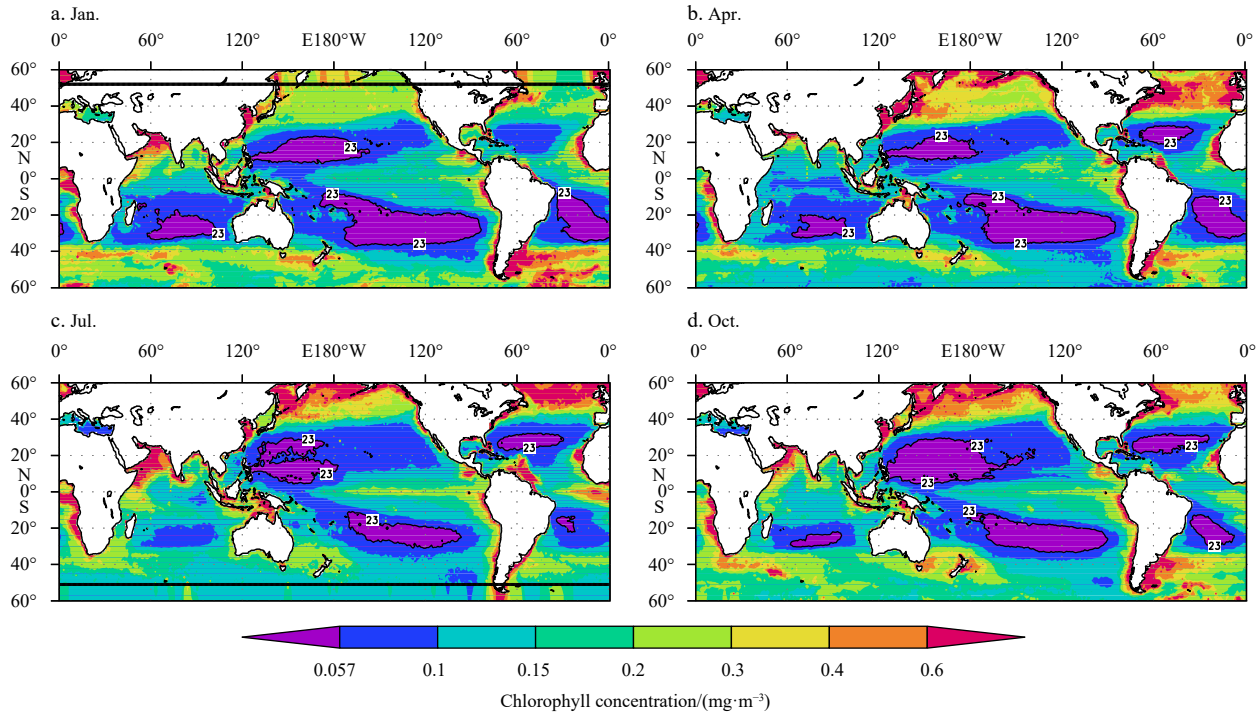

Fig. 1. Climatological mean of the chlorophyll concentration (shaded) and the 23 m attenuation depth of the visible and ultraviolet bands (contours, m) in January (a), April (b), July (c) and October (d). The chlorophyll data are from the SeaWiFS ocean color data from 1997 to 2007. The attenuation depth was computed using the method of Ohlmann (2003), in which the four parameters are all functions of chlorophyll concentration. The chlorophyll concentration north of 51°N in January and south of 51°S in July was interpolated by Kriging interpolation; and 51°S lines are indicated by thick black lines.

(CIAF) and Corrected Normal Year Forcing (CNYF) of the Common Ocean-ice Reference Experiments (CORE) dataset (Large and Yeager, 2004). The datasets were regridded to the grid of the ocean general circulation model via the linear-interpolation method.

2.2 *Model description*

The model used in this study is the State Key Laboratory of Numerical Modeling for Atmospheric Sciences and Geophysical Fluid Dynamics (LASG)/Institute of Atmospheric Physics (IAP) Climate System Ocean Model (LICOM), version 2 (Liu et al., 2004a, b, 2012b). LICOM is an ocean general circulation model and is the oceanic component of the Flexible Global Ocean–Atmosphere–Land System (FGOALS) model, version 1 (Yu et al., 2004) and version 2 (Lin et al., 2013a, b). The longitudinal resolution of LICOM in the present study is 1°. The meridional resolution between 10°S and 10°N increases to 0.5°, and then gradually decreases to 1° at 20° (N/S). The model has 15 uniform 10 m levels in the upper ocean and 15 nonuniform levels below 150 m.

A two-exponential formula is employed to describe the penetration of solar radiation in LICOM:

$$Q_z = Q_0 \left(A_1 \mathrm{e}^{-\frac{z}{B_1}} + A_2 \mathrm{e}^{-\frac{z}{B_2}} \right), \tag{1}$$

where Q_z and Q_0 represent the downward solar radiation penetrating at a certain depth (z), and the net solar radiation at the surface, respectively. The terms A_1 (A_2) and B_1 (B_2) represent the fraction of the total solar flux that resides in the infrared band (ultraviolet and visible bands) and its penetration depth, respectively. The infrared band (first term) is usually absorbed in the upper 1 m, which is much smaller than the thickness of the first layer (10 m); the visible-ultraviolet band (second term) can penetrate below 50 m in clear water. Thus, the variation in the penetration of solar radiation in the model is primarily caused by variations in the e-folding attenuation depth of the visible-ultraviolet band (B_2).

A global configuration of LICOM is employed in the present study. The model was first integrated for 100 years using observational salinity and temperature data, forced by the CORE CNYF dataset (Large and Yeager, 2004). Then, two 18-year integrations (1990–2007) were run, forced by the daily mean atmospheric variables from the CIAF of the CORE dataset. The only differences between the two experiments are the solar radiation penetration schemes. In the control run, the parameters of the two terms are assigned to constants following the method of Jerlov (1968) (hereafter referred to as CONTROL). A_1, A_2, B_1 and B_2 were set to 0.58, 0.42, 1 m and 23 m, respectively. The solar radiation is absorbed in the upper 1 m due to the infrared band and is absorbed below the surface in the ultraviolet and visible bands within the attenuation depth of 23 m. In the sensitivity run, the scheme proposed by Ohlmann (2003) was employed to represent the influence of the chlorophyll concentration on the penetration of solar radiation (hereafter referred to as CLIMCHL). Here, all four parameters are functions of the chlorophyll concentration, which can be found in Table 1 of Ohlmann (2003).

The chlorophyll data used in the CLIMCHL run are the climatological monthly mean. The effects of chlorophyll heating were investigated by comparing the two runs. In the CLIMCHL run, the 23 m attenuation depth approximately corresponds to a chlorophyll concentration of 0.057 mg/m^3. Within the contours of the 23 m attenuation depth in Fig. 1, the chlorophyll concentration is less than 0.057 mg/m^3 and the solar radiation can penetrate deeper than 23 m. Thus, less solar radiation will be absorbed by the upper layer in the CLIMCHL run than in the CONTROL run. In the regions outside the 23 m attenuation depth contours, the e-folding depth is shallower than 23 m. Therefore, more solar radiation will be absorbed by the upper layer in the CLIMCHL run than in the CONTROL run and less solar radiation will penetrate below.

2.3 *Model validation*

To evaluate the performance of LICOM, we first compared the simulated SST from CONTROL with the observations from WOA13 (Fig. 2). The SST of WOA show large variation both in the tropic and the extratropic. LICOM could reproduces the seasonal

Table 1. Classification of each region and summary of the dominant heat budget mechanisms of each region

Region	Longitude and latitude range	Classification	Balance (warming~cooling)
1	15°–25°N, 150°–170°E	attenuation depths greater than 23 m	Qnet~Qpen
2	24°–32°N, 40°–70°W		
3	20°–28°S, 115°–145°W		
4	10°–20°N, 50°–60°E	tropical coastal upwelling regions	Ent (w_b)~Qnet + Qpen
6	12°–25°S, 8°–15°E		
7a	8°–15°S, 75°–85°W		
5	16°–25°N, 15°–20°W	mid-latitudes upwelling regions	Ent (w_b) + Adv-u ~ Qpen
7b	35°–45°S, 72°–80°W		
8	5°S–5°N, 100°–140°W	equatorial upwelling region	Ent (w_b) + Adv-v ~ Qnet + Qpen
9	5°S–5°N, 0°–30°W		
10	35°–45°N, 160°E–140°W	mid-latitudes	Qnet + Adv ~ Qpen
11	35°–45°S, 50°–110°E		
12	38°–48°S, 110°–160°W		
13	38°–48°S, 0°–40°W		
14	20°–25°N, 60°–70°E	special regions	Ent (dhdt) + Qnet~ Qpen + R
15	35°–45°N, 10°–30°W		
16	35°–45°S, 72°–80°W		

Note: These regions are marked in Fig. 4 in different colors. Ent (w_b) indicates the contribution is from the enhanced vertical velocity at the base of the mixed layer w_b and Ent (dhdt) means that the contribution is from the quick deepening of the MLD. Adv-u and Adv-v are the zonal and meridional horizontal advection, respectively. Qnet and Qopen are the net surface heat flux and the downward radiative flux at the bottom of the mixed layer, respectively.

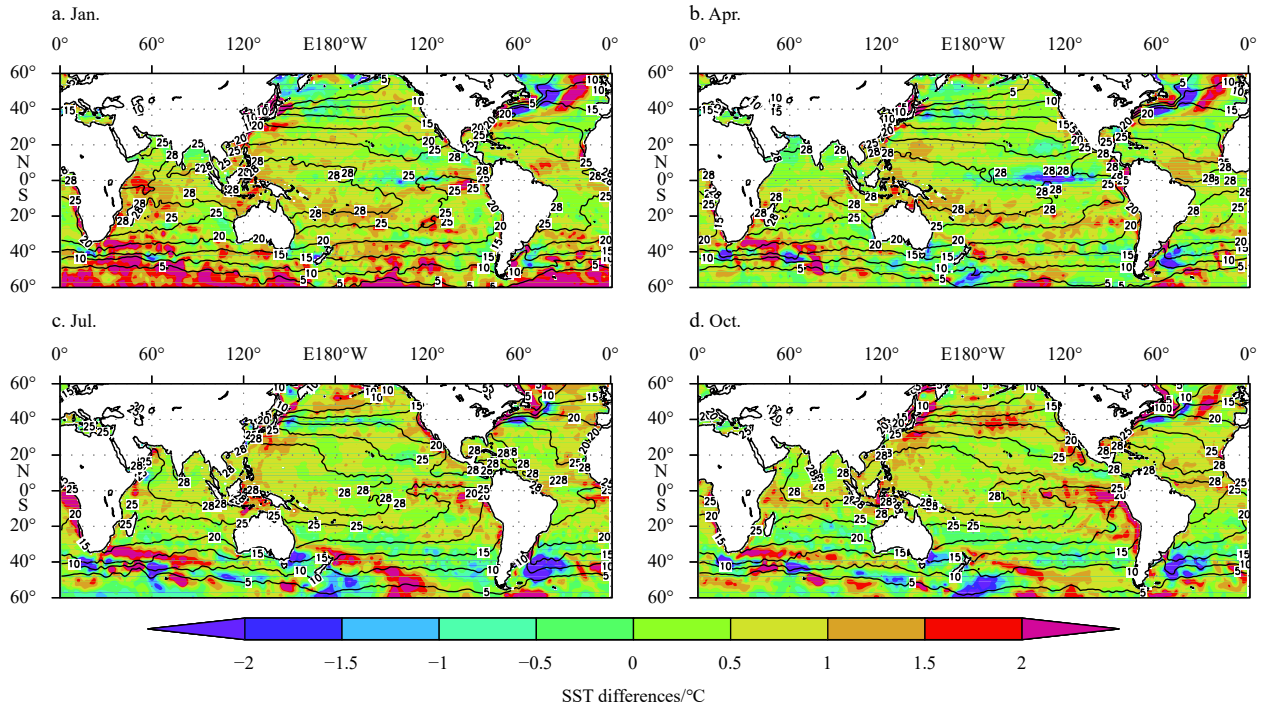

Fig. 2. Seasonal variation in SST for January (a), April (b), July (c) and October (d). The contours show the SST (℃) from WOA13 and the shading shows the SST differences between the LICOM CONTROL run and WOA13.

variation of the SST. There are significant warming biases (larger than 2°C) in the mid-latitudes (poleward of 40°), both in the North Atlantic Ocean and the Southern Hemisphere, especially in boreal winter. There are significant cooling biases in the eastern equatorial Pacific region during boreal spring (Figs 2a and b). The averaged SST in the tropical region is 26.70°C and 27.38°C for WOA and LICOM, respectively. In the Northern Hemisphere, the averaged SST in the mid-latitudes (30°–60°N) is 13.98°C and 14.78°C for WOA and LICOM, respectively, and in the southern mid-latitude (30°–60°S) it is 11.07°C and 11.58°C, respectively. In general, the modeled SST is a little warmer than the observed SST. However, comparing the differences between experiments,

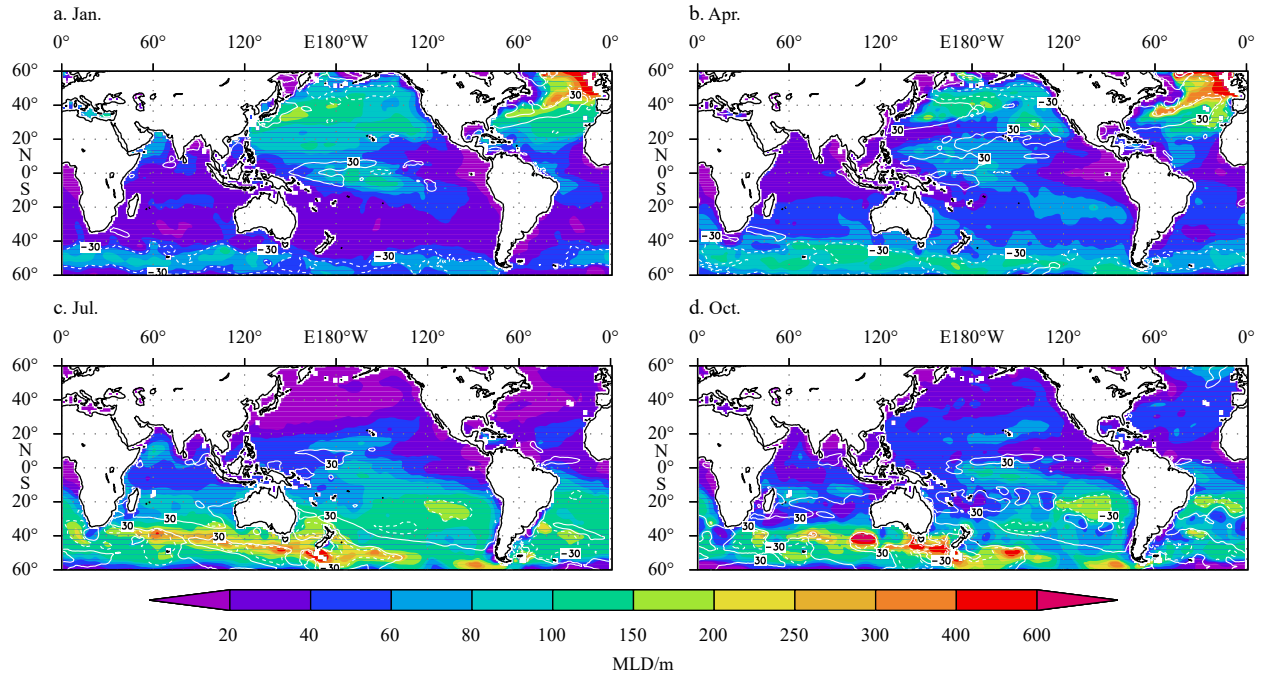

Fig. 3. Seasonal variation in the MLD for January (a), April (b), July (c) and October (d). The shading shows the MLD from WOA13 and the contours show the MLD differences between the LICOM CONTROL run and WOA13. Dotted white lines show the –30 m MLD differences and solid white lines show 30 m MLD differences.

it is likely that the systematic biases of the model will be greatly reduced.

The MLD of LICOM was also validated against that of WOA13 (Fig. 3). Here, the MLD is defined as the depth with a potential density equivalent to a specific density that is computed using the sea surface salinity and SST $-\Delta T$. Here, we selected ΔT = 0.8°C following the methods of Kara et al. (2000) and Du et al. (2005). The MLD shows significant seasonal variation, especially in the mid-latitudes, from approximately several tens of meters in local summer to several hundreds of meters in local winter. In boreal winter and spring (Figs 3a and b), LICOM tends to simulate thinner MLDs approximately 50°N and 50°S (greater than 30 m), and thicker MLDs approximately 30°–40°N (greater than 30 m). In austral winter and spring (Figs 3c and d), there are both thinner and thicker biases in the Southern Hemisphere. The biases are oriented from northwest to southeast (with a maximum greater than 30 m). In the equatorial regions, LICOM tends to simulate thicker MLDs in the west in all seasons (greater than 30 m). The biological heating effect in the upper mixed layer will be underestimated with thicker MLDs and overestimated with thinner MLDs.

Although there are biases in the model results, LICOM reproduces the seasonal variation of the SST and MLD well. Additionally, given that we compared and computed the differences between experiments, these systematic biases of the two model experiments tend to be greatly offset. Thus, these biases will have a negligible effect on our conclusions and we deem the model suitable the present study.

2.4 *Mixed layer heat budget*

To understand the underlying mechanisms involved in the effects of biological heating, the mixed layer heat budget was calculated. The equation governing the mixed layer temperature is as follows (Du et al., 2005):

$$\frac{\partial T}{\partial t} = \frac{Q_0 - Q_h}{\rho C_p h} - \vec{V} \cdot \nabla T - \frac{w(T - T_d)}{h} + R, \tag{2}$$

where T is the mixed layer averaged temperature; Q_0 and Q_h are the net surface heat flux and the downward radiative flux at the bottom of the mixed layer, respectively; C_p is the specific heat capacity of sea water (3 996 J/(kg·K)); ρ is the seawater density (1 025 kg/m^3); h is the MLD; $\vec{V}$ is the horizontal velocity vector; w is the entrainment rate; T_d is the temperature just below the mixed layer; and R is the residual term. The entrainment rate, w, is defined as

$$w = \begin{cases} \dfrac{\partial h}{\partial t} + w_b + \vec{V} \cdot \nabla h, & \dfrac{\partial h}{\partial t} + w_b + \vec{V} \cdot \nabla h > 0, \\ 0, & \text{otherwise}, \end{cases} \tag{3}$$

where $\partial h/\partial t$ denotes the rate at which the mixed layer deepens; w_b is the vertical velocity at the base of the mixed layer, in which positive (negative) indicates upwards (downwards); and $\vec{V} \cdot \nabla h$ is the horizontal advection of water parcels in the mixed layer (hereafter referred to as Advh).

In the following, the term on the left-hand side of the heat budget equation (Eq. (2)) is referred to as the temperature tendency (dTdt) and the four terms on the right-hand side are referred to as the surface thermal forcing (Qhm), horizontal advection (Adv), entrainment (Ent), and residual (R). Qhm can be further decomposed into the net surface heat flux (Qnet) and the downward radiative flux at the bottom of the mixed layer (Qpen). These terms are calculated by the monthly model output and their relative importance was analyzed to elucidate the possible mechanisms involved in controlling the response of the upper layer to chlorophyll heating.

3 Results

3.1 *Temperature differences between the two experiments*

We first investigated the annual mean SST differences between the two experiments (Fig. 4a, CLIMCHL minus CONTROL). Negative SST differences could be seen in upwelling regions and all the subtropical gyres. Most other regions show weak positive SST differences. Compared to the seasonal SST differences (Figs 4b-e), the magnitude of annual mean SST differences are much weaker. As SST differences show strong seasonal variation, positive and negative values are offset in the annual mean. We will focus on the seasonal variation of the SST differences.

In regions where the attenuation depths are less than 23 m (outside of the 23 m contours in Fig. 4, with chlorophyll concentrations greater than 0.057 mg/m^3), solar radiation was absorbed more by the mixed layer in the CLIMCHL run than that in the CONTROL run. Therefore, there was biological warming in the mixed layer. At mid-latitudes (poleward of 30°), the SST in most regions was cooling (by approximately 0.2–0.8°C) in local winter and warming (by 0.2–0.8°C) in local summer in CLIMCHL (Figs 4b and d). The warming at mid-latitudes is caused by the absorption of heat by phytoplankton. The SST in the North Indian Ocean was cooling in boreal winter and summer (Figs 4b and d) and warming in boreal spring and autumn (Figs 4c and e). The SST differences in the Pacific Ocean, Atlantic Ocean and the South Indian Ocean were significantly negative in local winter and positive in local summer, with both warming and cooling differences in the transitional seasons (local spring and autumn). In the equatorial regions, both warming and cooling are apparent, with larger SST cooling differences in the upwelling regions (significant in the Pacific Ocean and Atlantic Ocean, weak in the Indian Ocean) in boreal summer (Fig. 4d).

Within regions where the attenuation depths are deeper than 23 m (within the 23 m contours in Fig. 4, chlorophyll concentrations less than 0.057 mg/m^3), the seasonal variations of the SST differences differed from those in regions with relatively higher chlorophyll concentrations (greater than 0.057 mg/m^3). The SST differences showed warming in local winter and cooling in the other seasons (Figs 4b-e).

The warming effects where the chlorophyll concentration is higher than 0.057 mg/m^3 are unsurprising. However, there are also cooling areas with biological heating. The cooling effects are related to different dynamic mechanisms (i.e., upwelling and mixing), as presented in previous studies (e.g. Liu et al., 2012a; Ma et al., 2012, 2014). We focus on these cooling regions and examine the underlying mechanisms involved by analyzing the mixed layer heat budget. As there are no chlorophyll concentration data north of 51°N in January and south of 51°S in July in SeaWiFS, we only examine regions within these bounds.

The distribution of the mixed layer averaged temperature differences is similar to that of the SST differences (figures not shown). As the effects of biological heating are also impacted by dynamic processes, we defined 17 regions (boxes in Figs 4b and d) according to their SST differences and dynamic features. As shown in Fig. 4, the attenuation depths are deeper than 23 m (blue boxes; regions 1, 2 and 3); upwelling dominates in coastal areas (orange boxes; regions 4, 6 and 7a in the tropics and re-

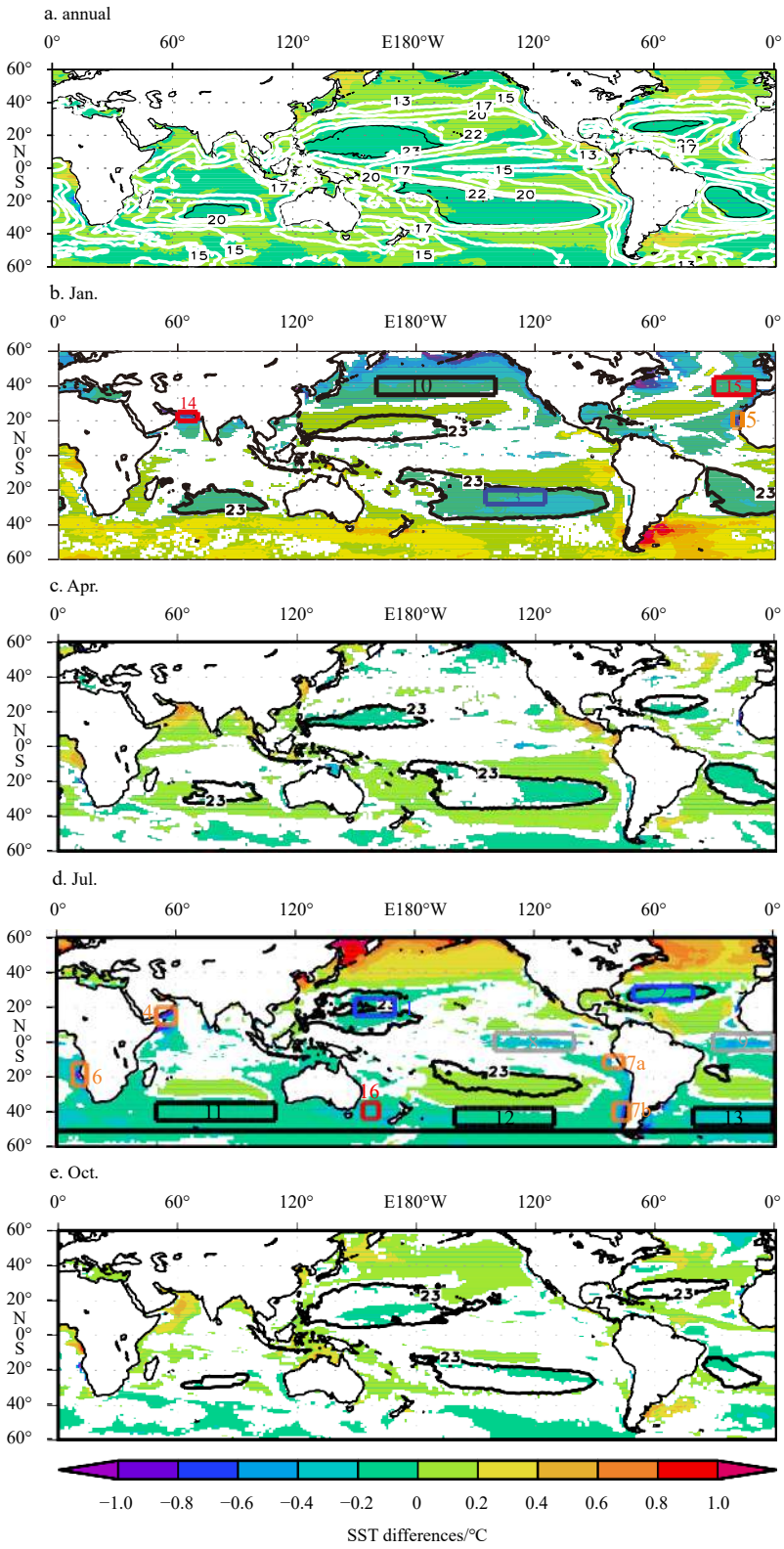

Fig. 4. Annual mean of SST difference between CLIMCHL and CONTROL runs (a). Figures b-e show SST differences between the CLIMCHL and CONTROL runs for January, April, July and October, respectively. The contours are the same as in Fig. 1. SST differences of less than one standard deviation have been removed. The black contours show the 23 m attenuation depth, and white contours show the attenuation depth shallower than 23 m.

gions 5 and 7b in the mid-latitudes) and equatorial areas (gray boxes; regions 8 and 9); strong mixing occurs in the mid-latitudes in local winter (black boxes; regions 10, 11, 12 and 13); and significant negative SST differences are apparent, but not for any of the aforementioned factors (red boxes; regions 14, 15 and 16). The longitudes and latitudes of the domains are listed in Table 1.

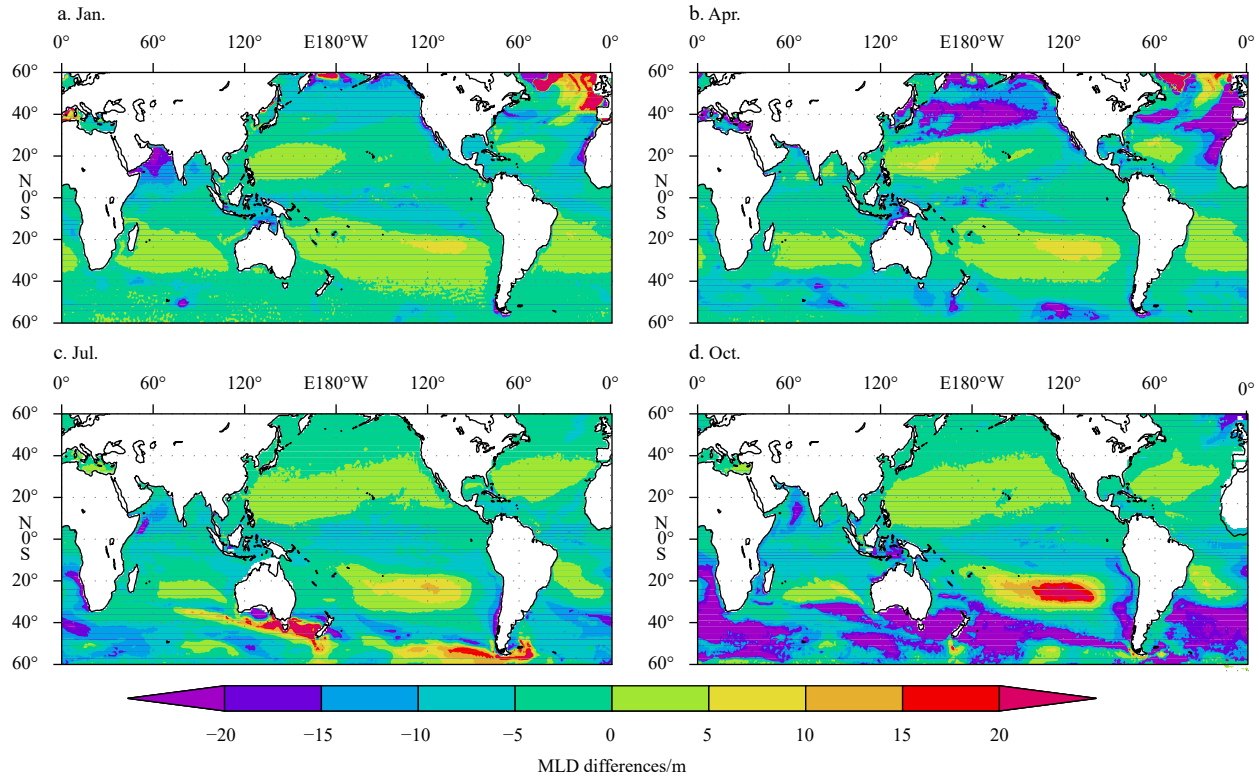

Fig. 5. MLD differences between the CLIMCHL and CONTROL runs for January (a), April (b), July (c) and October (d).

The mixed layer heat budget analysis is analyzed for each region in the following subsections. In most regions, the ML in CLIMCHL is shallower than that of CONTROL, except for regions where the attenuation depths are deeper than 23 m and regions with very strong mixing such as the northern North Atlantic Ocean in boreal winter and spring and some regions between 40°S and 60°S during austral winter (Fig. 5). As the MLD is very deep in regions with strong mixing, according to Eq. (2), when divided by the MLD, the Qhm and Ent terms are small, so the deepened MLD does not significantly affect the results.

3.2 *Regions with attenuation depths greater than 23 m (regions 1, 2 and 3)*

Regions 1, 2 and 3 lie in the subtropical gyres, and attenuation depths greater than 23 m. In these regions, the energy absorbed in the upper layer in the CLIMCHL run is less than that in the CONTROL run. The SST differences are opposite in the two hemispheres, with positive (negative) differences in the winter (summer) hemisphere. We chose to study regions 1 and 2 in the Northern Hemisphere and region 3 in the Southern Hemisphere, as shown in Fig. 4. Our analysis focuses on periods when negative temperature tendency (dTdt) occurred.

The mixed layer heat budget differences in regions 1 and 2 show that dTdt clearly cooled for several months before June and reaches a negative maximum in boreal spring (figures not shown). Therefore, the SST differences are negative in boreal spring and summer (Fig. 4). In the Southern Hemisphere, the situation for region 3 is similar to that of regions 1 and 2, but the large cooling season appears in austral summer (Fig. 4b) and the maximum negative dTdt difference occurs in austral spring (figures not shown).

To further investigate the reasons for cooling, Qhm was decomposed into the net surface heat flux (Qnet) and downward radiative flux at the bottom of the mixed layer (Qpen), based on Eq. (2). Qnet and Qpen are equal to $Q_0/\rho C_p h$ and $-Q_h/\rho C_p h$, respectively. The net surface heat flux, Q_0, is mainly dominated by the shortwave radiation and latent heat flux, and the penetration of shortwave radiation, Q_h, is affected by the perturbation of chlorophyll. Variations in Qnet and Qpen are also related to variations in the MLD, h. We chose the period from April to June for regions 1 and 2 and from October to December for region 3 (Fig. 6). The balance is mainly between Qnet cooling and Qpen warming for these regions. Although the shortwave radiation is strong in local spring and summer, the latent heat flux of CLIMCHL is less than that of CONTROL (data not shown) because the SST of CLIMCHL is colder than that of CONTROL. As a result, the Q_0 for CLIMCHL is greater than that of CONTROL. However, the MLD of CLIMCHL is greater in these regions (Fig. 5), which leads to a negative Qnet difference (cooling effect). As the radiation usually reduced to 1% of the surface radiation even at depth of 20–30 m. The deep MLD (around 100 m) in both experiments during summer means that the Q_h differences for both experiments can be neglected. The greater MLD of CLIMCHL leads to a positive Qpen difference (Fig. 6), which plays a warming role. Therefore, the cooling in these regions is due to the large heat capacities of the thicker mixed layer, which prevent the temperature from increasing as fast as that in a thinner mixed layer.

3.3 *Regions of upwelling*

3.3.1 *Tropical coastal upwelling regions (regions 4, 6 and 7a)*

We chose three tropical coastal upwelling regions with significant negative SST differences: region 4 (western Arabian Sea) in the Northern Hemisphere and regions 6 (west coast of South Africa) and 7a (west coast of South America) in the Southern Hemisphere. Upwelling occurs during boreal summer in regions

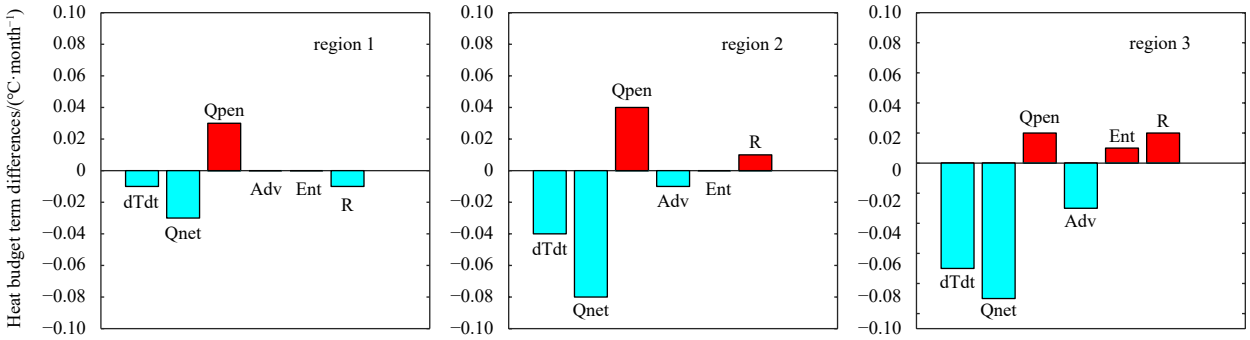

Fig. 6. Histogram of the heat budget term differences for the upper mixed layer between the CLIMCHL and CONTROL runs for regions 1, 2 and 3. dTdt is the temperature tendency; Qnet is net surface heat flux and Qpen is the downward radiative flux at the bottom of the mixed layer; Adv is the horizontal advection; Ent is the vertical entrainment; and R stands for the residual term. All the terms are averaged from April to June for regions 1 and 2 and from October to December for region 3 when dTdt is negative.

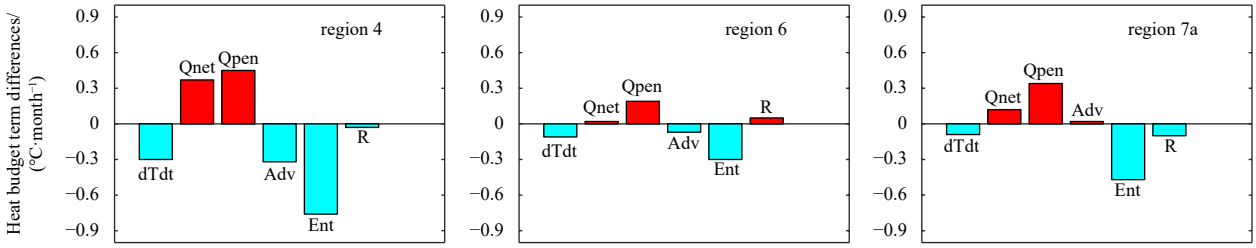

Fig. 7. As in Fig. 6 but for the tropical coastal upwelling regions (regions 4, 6 and 7a). The heat budget term differences are all outside the 23 m attenuation depth contours. All terms are averaged from May to July when dTdt is negative.

4, 6 and 7a. The differences in the dTdt show a weak cooling tendency before July in regions 4, 6 and 7a (figures not shown), which leads to cooling SST differences during boreal summer. We chose the period from May to July for analysis (Fig. 7). The heat budget analysis shows that the balances are mainly between the Qnet and Qpen heating terms and Ent cooling term. In regions 4 and 6, the Adv differences also show a clear cooling effect. When Qnet and Qpen heating are unable to cancel out the cooling caused by Ent (and Adv for region 4), negative dTdt occurs, which ultimately leads to negative SST differences, i.e., during boreal summer in regions 4, 6 and 7a (Fig. 4).

Because there is little difference in Q_0 in the two runs during the study period, the shallower MLD in the CLIMCHL run leads to positive Qnet differences (warming effect). The Q_h for CLIMCHL is smaller than that of CONTROL, leading to a positive Qpen difference (warming effect). The vertical velocity differences at the base of the mixed layer, w_b, contribute mostly to the Ent differences in these regions (about –0.5°C/month to –1°C/month). In upwelling regions, the upward velocity for the CLIMCHL run is enhanced, which could bring the colder subsurface water to the surface and cool the SST. Zonal advection (Adv-u) contributes mostly to the horizontal advection for regions 4 and 6 (about –0.2°C/month to –0.5°C/month). Offshore current differences at the surface (figures not shown) transport the cooling water away from the coast, which leads to more subsurface colder water moving upwards to supply the surface and cool the SST. In Liu et al. (2012a), the cooling mechanism identified for the Java coast is similar to that in the regions mentioned in this subsection, although it is not as significant as in the coastal upwelling regions above.

3.3.2 *Mid-latitude upwelling regions (regions 5 and 7b)*

We chose region 5 in the Northern Hemisphere and region 7b in the Southern Hemisphere (southwest of South America). Both regions show cooling during the local winter. The differences in dTdt show a weak-cooling tendency during local winter in both regions. We chose the negative dTdt period from November to January and April to July for region 5 and region 7b, respectively.

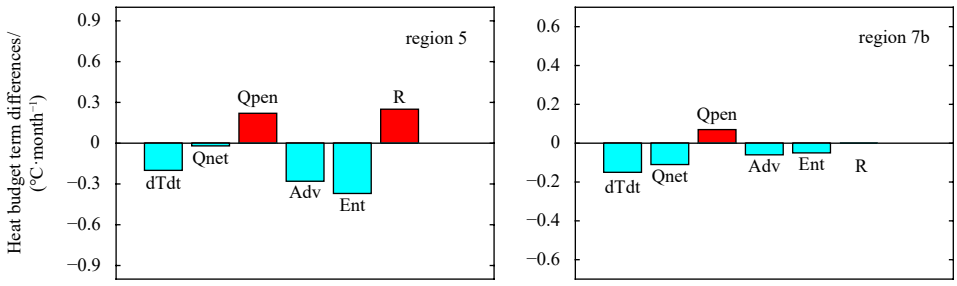

Fig. 8. As in Fig. 7 but for the mid-latitude upwelling regions (regions 5 and 7b). The terms are averaged from November to January for region 5 and April to June for region 7b when dTdt is negative.

Heat budget analysis shows that the balances are mainly between the Qpen heating term and the Qnet, Ent and Adv cooling terms (Fig. 8). When Qpen heating are unable to cancel out the cooling caused by Qnet, Ent and Adv, negative dTdt occurs, which ultimately leads to negative SST differences.

Different from the tropical upwelling regions in Section 3.3.1, Qnet has cooling effect in the mid-latitudes upwelling region. Q_0 is negative for CLIMCHL and CONTROL during local winter (figures not shown), combined with shallower MLD in CLIMCHL run (Fig. 5), leading to a negative Qnet difference (cooling effect). The Q_h for CLIMCHL is less than that for CONTROL, leading to a positive Qpen difference (warming effect). Similar to the tropical upwelling regions, the vertical velocity differences at the base of the mixed layer, w_b, contribute mostly to the Ent differences in these two regions (figures not shown). Zonal advection (Adv-u) and meridional advection (Adv-v) contributes mostly to the horizontal advection for regions 5 and 7b, respectively (figures not shown).

3.3.3 *Equatorial upwelling regions (regions 8 and 9)*

As the cooling SST differences in the tropical eastern Indian Ocean are not very significant in all four seasons, we chose regions in the equatorial Pacific Ocean (region 8) and Atlantic Ocean (region 9) for analysis. The situations in these two regions are similar. As the dTdt differences are negative before July (figures not shown), the negative SST differences are most significant in July (Fig. 4). We chose the negative dTdt period from May to July for analysis. The heat budget analysis shows that the balances are mainly between Qnet and Qpen warming and Ent and Adv cooling (Fig. 9).

The Qhm heating term differences are positive all year round. The differences in Qhm are primarily dominated by the differences in Qnet and secondarily contributed by Qpen differences, which are caused by the existence of chlorophyll. The warming effects of Qnet and Qpen are similar to those in the coastal upwelling region. The Ent differences are also mainly caused by the w_b differences in the equatorial upwelling region (figures not shown). Enhanced w_b reveals a strengthened upward velocity for the CLIMCHL run, which could bring the colder subsurface water to the surface and cool the SST. The negative Adv differences are mainly caused by poleward meridional advection (Adv-v) (figures not shown). Similar to the offshore currents in the coastal region, the off-equator surface current differences (figures not shown) will transport the cooling surface water away from the equator, which will lead to more subsurface colder water moving upwards to supply the surface water and cool the SST. In summary, in the equatorial upwelling region, the entrainment caused by the upward velocity and poleward meridional advection cancel out the Qnet and Qpen heating and lead to a cooler SST.

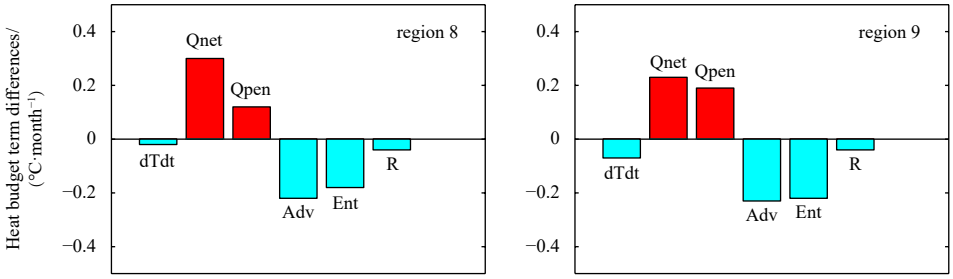

Fig. 9. As in Fig. 7 but for the equatorial upwelling regions (regions 8 and 9). The terms are averaged from May to July when dTdt is negative.

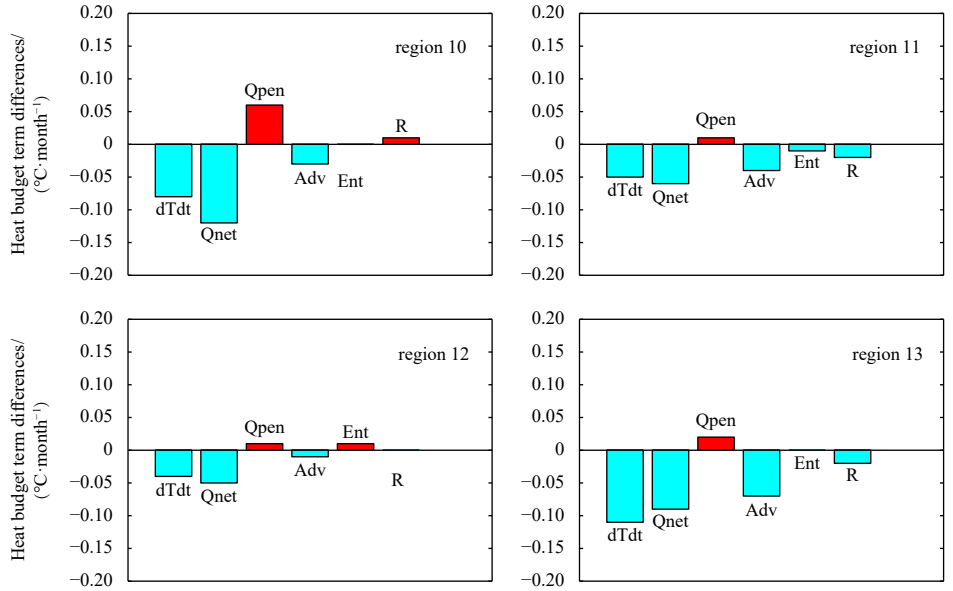

Fig. 10. As in Fig. 7 but for the mid-latitude poleward of 35°N and 35°S (regions 10, 11, 12 and 13). The terms are averaged from October to December for region 10 and April to June for regions 11–13 when dTdt is negative.

3.4 *Regions in the mid-latitudes (regions 10, 11, 12 and 13)*

We chose region 10 in the Northern Hemisphere and regions 11, 12 and 13 in the Southern Hemisphere. The MLD in the mid-latitudes can reach up to several hundreds of meters in local winter due to large heat loss. According to Eq. (2), if the MLD is thick, there will be few differences between each term. The SST differences show clear cooling effects during local winter for each region. The differences in the dTdt show a clear cooling tendency before local winter in all four regions (data not shown). We chose the negative dTdt period from October to December for region 10 and from April to June for regions 11–13. The heat budget analysis shows that the balances are mainly between Qpen warming and Qnet and Adv cooling (Fig. 10).

The negative Adv differences are mainly caused by meridional advection (Adv-v) (data not shown). There is not much difference in the Q_0 (negative) of CLIMCHL and CONTROL during local winter (data not shown). However, the MLD is shallower in the CLIMCHL run (Fig. 5), which leads to a negative Qnet difference (cooling effect). Because the chlorophyll concentration is still high during late autumn in CLIMCHL, the Q_h is less than that of the CONTROL. Combining with the MLD leads to positive Qpen differences (warming effect), which means that more heat is trapped in the upper layer. Although the Qpen differences constitute a warming effect, they are very weak and cannot cancel out the cooling of Qnet and Adv, and the dTdt differences turn negative several months before December in region 10 in the Northern Hemisphere and before July in regions 11, 12 and 13 in the Southern Hemisphere. As a result, the SST differences show significant cooling in local winter in these regions (Fig. 4).

3.5 *Special regions (regions 14, 15 and 16)*

In addition to the regions analyzed above, we also selected three special regions: region 14 in the northern Arabian Sea, region 15 west of Europe, and region 16 southeast of Australia. There is no upwelling in these regions, and significant cooling SST differences occur in local winter. Although these regions are distributed at different latitudes and in different oceans, the heat budget analysis shows a similar mechanism. The differences of dTdt show a clear cooling tendency before local winter in all three regions (figures not shown). We analyzed the negative dTdt period from October to December for regions 14 and 15 and from May to July for region 16. The heat budget analysis shows that the balances are mainly between R warming and Qnet and Ent cooling (Fig. 11).

In contrast to the mid-latitude regions in Section 3.4, both Ent and Qnet are cooling terms in local winter (Fig. 11), which are balanced by R warming. The Ent differences are contributed by dhdt (Fig. 11), which is caused by the more rapid increase in the MLD of the CLIMCHL run (data not shown); this is different from the situation in the upwelling regions, where the contribution is from w_b. According to Eq. (1), if the MLD is thick in winter, there will be little difference in the downward radiative flux at the bottom of the mixed layer (Qpen) between the two runs. Q_0 was negative during local winter and the absolute Q_0 of the CLIMCHL run was less than that of CONTROL run but combined with MLD, leading to negative Qnet differences.

4 Summary and discussion

The present study investigates the biological effects on SST in the global ocean by using an ocean general circulation model. Based on the mixed layer heat budget, the physical mechanisms are analyzed by comparing two experiments with and without chlorophyll concentrations. The biological heating is a thermodynamic process and involves ocean dynamic processes such as changing circulation and MLD. We selected 17 regions for analysis, including 14 regions where the chlorophyll concentrations are higher than the reference value (0.057 mg/m^3), and found SST is cooling instead of warming in certain seasons. We classified these regions according to their dynamic processes, as ocean dynamics impact the warming or cooling effects of the chlorophyll concentration. We obtained a global view of the biological effects. SST warming will appear in regions with shallow mixed layer during the period from local spring to autumn and SST cooling will appear in regions experiencing strong upwelling (usually during local summer and autumn) and strong mixing (usually during local winter). The results of the heat budget analysis are summarized in Table 1.

In regions with attenuation depths greater than 23 m (regions 1, 2, and 3), the SST differences are opposite in the two hemispheres, with positive (negative) differences in the winter (summer) hemisphere. The balance is mainly between Qnet cooling and Qpen warming for these regions.

In the tropical upwelling regions (region 4, region 6 and region 7a), SST differences show cooling effects during boreal summer. The heat budget analysis shows that the balances are mainly between the Qnet and Qpen heating term and Ent cooling terms. In the mid-latitude upwelling regions (region 5 and region 7b), SST differences show cooling effects during local winter. The heat budget analysis shows that the balances are mainly between the Qpen heating term and the Qnet, Ent and Adv cooling terms (Fig. 8). In the equatorial Pacific Ocean (region 8) and Atlantic Ocean (region 9), the negative SST differences are most significant in July. The heat budget analysis shows that the balances are mainly between Qnet and Qpen warming and Ent and Adv cooling (Fig. 9). The Ent cooling effects in the upwelling regions above are caused by the enhanced vertical velocity at the base of the mixed layer, w_b.

In the mid-latitudes (regions 10–13), the SST differences show clear cooling effects during local winter for each region. The balances are mainly between Qpen warming and Qnet and Adv

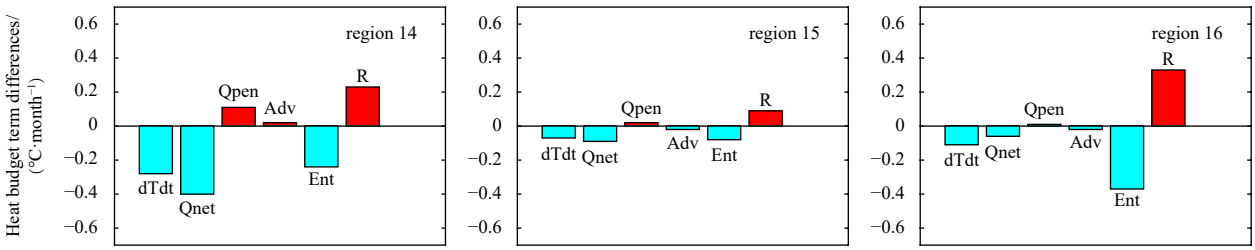

Fig. 11. As in Fig. 7 but for the special regions (regions 14, 15 and 16). The terms are averaged from October to December for regions 14–15 and May to July for region 16 when dTdt is negative.

cooling. In some regions (regions 14–16) that do not belong to the categories above, significant cooling SST occurs in local winter. The balances are mainly between R warming and Qnet and Ent cooling. The Ent differences in these regions are contributed by dhdt, which is caused by the rapid increase in the MLD. This is different from the situation in the upwelling regions, where the contribution is from w_b.

In Section 3, we do not discuss the significant cooling regions northeast of the United States during boreal winter or southeast of South America during austral winter. These two cases belong to the western boundary currents and show some biases in the output of the present model. Our intention is to verify them in future work once the biases have been corrected.

The effects of biological heating on SST are expected to be enlarged when atmosphere–ocean coupled models are used (Lin et al., 2007; Gnanadesikan and Anderson, 2009). In most regions, the SST differences between experiments are opposite in the Southern and Northern Hemispheres (Fig. 4). The warming (cooling) effects in the Southern Hemisphere and cooling (warming) effects in the Northern Hemisphere in boreal winter (summer) might change the meridional atmospheric circulation in atmosphere–ocean coupled models, e.g., the warming approximately 30° and cooling at the tropics in both hemispheres in local winter might weaken the Hadley circulation (Fig. 4d). In addition, the persistent negative SST difference in the eastern tropical Pacific might strengthen the Walker circulation. These changes in atmospheric circulation might enhance the SST differences until reaching a balance.

As chlorophyll concentrations may respond to changes in the physical environment, feedback occurs between the biological and physical processes taking place. Manizza et al. (2005) noted that positive feedback occurs between phytoplankton dynamics, SST, sea-ice cover and solar radiation. During summer, a phytoplankton bloom can warm the surface and lead to sea-ice melting. Thus, the sea-ice cover is reduced and more solar radiation can reach the surface and further enhance the growth of phytoplankton. This positive feedback process could only be examined using a coupled ocean–biogeochemical model.

The present study has other limitations such as the coarse resolution (no eddies) and biases in the western boundary currents. More processes should be considered in future research to better understand the effects of biological heating.

Acknowledgements

We acknowledge the technical support from the National Key Scientific and Technological Infrastructure Project “Earth System Science Numerical Simulator Facility” (Earth Lab).

References

Anderson W G, Gnanadesikan A, Hallberg R, et al. 2007. Impact of ocean color on the maintenance of the Pacific Cold Tongue. Geophysical Research Letters, 34(11): L11609, doi: 10.1029/2007GL030100

Ballabrera-Poy J, Murtugudde R, Zhang Ronghua, et al. 2007. Coupled ocean–atmosphere response to seasonal modulation of ocean color: impact on interannual climate simulations in the Tropical Pacific. Journal of Climate, 20(2): 353–374, doi: 10.1175/JCLI3958.1

Du Yan, Qu Tangdong, Meyers G, et al. 2005. Seasonal heat budget in the mixed layer of the southeastern tropical Indian Ocean in a high-resolution ocean general circulation model. Journal of Geophysical Research: Oceans, 110(C4): C04012

Gnanadesikan A, Anderson W G. 2009. Ocean water clarity and the ocean general circulation in a coupled climate model. Journal of Physical Oceanography, 39(2): 314–332, doi: 10.1175/2008JPO3935.1

Jerlov N G. 1968. Optical Oceanography. Amsterdam: Elsevier, 194

Jochum M, Yeager S, Lindsay K, et al. 2010. Quantification of the feedback between phytoplankton and ENSO in the community climate system model. Journal of Climate, 23(11): 2916–2925, doi: 10.1175/2010JCLI3254.1

Kang Xianbiao, Zhang Ronghua, Gao Chuan, et al. 2017. An improved ENSO simulation by representing chlorophyll-induced climate feedback in the NCAR Community earth system model. Scientific Reports, 7: 17123, doi: 10.1038/s41598-017-17390-2

Kara A B, Rochford P A, Hurlburt H E. 2000. An optimal definition for ocean mixed layer depth. Journal of Geophysical Research: Oceans, 105(C7): 16803–16821, doi: 10.1029/2000JC900072

Large W, Yeager S. 2004. Diurnal to decadal global forcing for ocean and sea-ice models: the data sets and flux climatologies. NCAR technical note NCAR/TN-460+STR Technical Report, 105, doi: 10.5065/D6KK98Q6.NationalCenterforAtmosphericResearch,Boulder,Colo

Lengaigne M, Menkes C, Aumont O, et al. 2007. Influence of the oceanic biology on the tropical Pacific climate in a coupled general circulation model. Climate Dynamics, 28(5): 503–516, doi: 10.1007/s00382-006-0200-2

Lewis M R, Carr M E, Feldman G C, et al. 1990. Influence of penetrating solar radiation on the heat budget of the Equatorial Pacific Ocean. Nature, 347(6293): 543–545, doi: 10.1038/347543a0

Lewis M R, Cullen J J, Platt T. 1983. Phytoplankton and thermal structure in the Upper ocean: consequences of nonuniformity in chlorophyll profile. Journal of Geophysical Research: Oceans, 88(C4): 2565–2570, doi: 10.1029/JC088iC04p02565

Lin Pengfei, Liu Hailong, Zhang Xuehong. 2007. Sensitivity of the upper ocean temperature and circulation in the equatorial pacific to solar radiation penetration due to phytoplankton. Advances in Atmospheric Sciences, 24(5): 765–780, doi: 10.1007/s00376-007-0765-7

Lin Pengfei, Yu Yongqiang, Liu Hailong. 2013a. Long-term stability and oceanic mean state simulated by the coupled model FGOALS-s2. Advances in Atmospheric Sciences, 30(1): 175–192, doi: 10.1007/s00376-012-2042-7

Lin Pengfei, Yu Yongqiang, Liu Hailong. 2013b. Oceanic Climatology in the Coupled Model FGOALS-g2: Improvements and Biases. Advances in Atmospheric Sciences, 30(3): 819–840, doi: 10.1007/s00376-012-2137-1

Liu Hailong, Ma Jinfeng, Lin Pengfei, et al. 2012a. Numerical study of the effects of ocean color on the sea surface temperature in the southeast tropical Indian Ocean: the role of the barrier layer. Environmental Research Letters, 7(2): 024010, doi: 10.1088/1748-9326/7/2/024010

Liu Hailong, Lin Pengfei, Yu Yongqiang, et al. 2012b. The baseline evaluation of LASG/IAP Climate system Ocean Model (LICOM) version 2. Acta Meteorologica Sinica, 26(3): 318–329, doi: 10.1007/s13351-012-0305-y

Liu Hailong, Yu Yongqiang, Li Wei, et al. 2004a. Manual for LASG/IAP Climate system Ocean Model (LICOM1.0). Beijing: Science Press, 128

Liu Hailong, Zhang Xuehong, Li Wei, et al. 2004b. An eddy-permitting oceanic general circulation model and its preliminary evaluation. Advances in Atmospheric Sciences, 21(5): 675–690, doi: 10.1007/BF02916365

Locarnini R A, Mishonov A V, Antonov J I, et al. 2013. World Ocean Atlas 2013, Volume 1: Temperature. NOAA Atlas NESDIS 73, 40

Löptien U, Eden C, Timmermann A, et al. 2009. Effects of biologically induced differential heating in an eddy-permitting coupled ocean-ecosystem model. Journal of Geophysical Research: Oceans, 114(C6): C06011

Ma Jinfeng, Liu Hailong, Zhan Haigang, et al. 2012. Effects of chlorophyll on upper ocean temperature and circulation in the upwelling regions of the South China Sea. Aquatic Ecosystem Health & Management, 15(2): 127–134

Ma Jinfeng, Liu Hailong, Lin Pengfei, et al. 2014. Seasonality of biological feedbacks on sea surface temperature variations in the Ar-

abian Sea: The role of mixing and upwelling. Journal of Geophysical Research: Oceans, 119(11): 7592–7604, doi: 10.1002/2014JC010186

Ma Jinfeng, Liu Hailong, Lin Pengfei, et al. 2015. Effects of the interannual variability in chlorophyll concentrations on sea surface temperatures in the east tropical Indian Ocean. Journal of Geophysical Research: Oceans, 120(10): 7015–7027, doi: 10.1002/2015JC010862

Manizza M, Le Quéré C, Watson A J, et al. 2005. Bio-optical feedbacks among phytoplankton, upper ocean physics and sea-ice in a global model. Geophysical Research Letters, 32(5): L05603

Marzeion B, Timmermann A, Murtugudde R, et al. 2005. Biophysical Feedbacks in the Tropical Pacific. Journal of Climate, 18(1): 58–70, doi: 10.1175/JCLI3261.1

Murtugudde R, Beauchamp J, McClain C R, et al. 2002. Effects of penetrative radiation on the upper tropical ocean circulation. Journal of Climate, 15(5): 470–486, doi: 10.1175/1520-0442(2002)015<0470:EOPROT>2.0.CO;2

Nakamoto S, Kumar S P, Oberhuber J M, et al. 2001. Response of the equatorial Pacific to chlorophyll pigment in a mixed layer isopycnal ocean general circulation model. Geophysical Research Letters, 28(10): 2021–2024, doi: 10.1029/2000GL012494

Ohlmann J C. 2003. Ocean radiant heating in climate models. Journal of Climate, 16(9): 1337–1351, doi: 10.1175/1520-0442(2003)16<1337:ORHICM>2.0.CO;2

Sathyendranath S, Gouveia A D, Shetye S R, et al. 1991. Biological control of surface temperature in the Arabian Sea. Nature, 349(6304): 54–56, doi: 10.1038/349054a0

Siegel D A, Ohlmann J C, Washburn L, et al. 1995. Solar radiation, phytoplankton pigments and the radiant heating of the equatorial Pacific warm pool. Journal of Geophysical Research: Oceans, 100(C3): 4885–4891, doi: 10.1029/94JC03128

Sweeney C, Gnanadesikan A, Griffies S M, et al. 2005. Impacts of shortwave penetration depth on large-scale ocean circulation and heat transport. Journal of Physical Oceanography, 35(6): 1103–1119, doi: 10.1175/JPO2740.1

Tian Feng, Zhang Ronghua, Wang Xiujun. 2020. Effects on ocean biology induced by El Niño-accompanied positive freshwater flux anomalies in the tropical Pacific. Journal of Geophysical Research: Oceans, 125(1): e2019JC015790

Wetzel P, Maier-Reimer E, Botzet M, et al. 2006. Effects of ocean biology on the penetrative radiation in a coupled climate model. Journal of Climate, 19(16): 3973–3987, doi: 10.1175/JCLI3828.1

Wu Yongsheng, Tang C C L, Sathyendranath S, et al. 2007. The impact of bio-optical heating on the properties of the upper ocean: A sensitivity study using a 3-D circulation model for the Labrador Sea. Deep-Sea Research Part II: Topical Studies in Oceanography, 54(23–26): 2630–2642

Yu Yongqiang, Zhang Xuehong, Guo Yufu. 2004. Global coupled ocean-atmosphere general circulation models in LASG/IAP. Advances in Atmospheric Sciences, 21(3): 444–455, doi: 10.1007/BF02915571

Zhang Ronghua. 2015. Structure and effect of ocean biology-induced heating (OBH) in the tropical Pacific, Diagnosed from a hybrid coupled model simulation. Climate Dynamics, 44(3): 695–715, doi: 10.1007/s00382-014-2231-4

Zhang Ronghua, Tian Feng, Wang Xiujun. 2018. Ocean chlorophyll-induced heating feedbacks on ENSO in a coupled ocean physics-biology model forced by prescribed wind anomalies. Journal of Climate, 31(5): 1811–1832, doi: 10.1175/JCLI-D-17-0505.1

Zhang Ronghua, Tian Feng, Zhi Hai, et al. 2019. Observed structural relationships between ocean chlorophyll variability and its heating effects on the ENSO. Climate Dynamics, 53(9): 5165–5186